A&A 480, 793–795 (2008)
DOI: 10.1051/0004-6361:20077823e

Astronomy & Astrophysics

Erratum

Massive star-formation in G24.78+0.08 explored through VLBI maser observations⋆

L. Moscadelli[1], C. Goddi[2], R. Cesaroni[1], M. T. Beltrán[3], and R. S. Furuya[4]

[1] INAF, Osservatorio Astrofisico di Arcetri, Largo E. Fermi 5, 50125 Firenze, Italy
e-mail: mosca@arcetri.astro.it
[2] Harvard-Smithsonian Center for Astrophysics, 60 Garden Street, Cambridge, MA 02138, USA
[3] Departament d'Astronomia i Meteorologia, Universitat de Barcelona, Av. Diagonal 647, 08028 Barcelona, Catalunya, Spain
[4] Subaru Telescope, National Astronomical Observatory of Japan, 650 North A'ohoku Place, Hilo, HI 96720, USA

A&A 472, 867–879 (2007), DOI: 10.1051/0004-6361:20077823

Key words. masers – stars: formation – ISM: kinematics and dynamics – errata, addenda

Owing to wrong input parameters of the script used to calculate the proper motions, the absolute velocities of the water masers detected towards the mm core G24 C were not corrected for the apparent (Galactic Rotation and solar) motion. This error affected only the water maser absolute velocities in core G24 C.

The last sentence of the "Abstract", resuming results obtained for core C, has been re-written. Figure 4 and Table 6 (the latter is only available in electronic form), where water maser absolute velocities in G24 C are shown and listed, have to be replaced with Fig. 4 and Table 6 given hereafter. Sections 3.4.4 and 6, which, respectively, describe the water maser velocity pattern in core C and propose a viable interpretation, have been entirely re-written and are reported in this erratum. In Sect. 7 ("Conclusions and Future Work"), only the last paragraph discussing the results obtained for core C has been re-written. For clearness, in the sections "Abstract" and "Conclusions and Future Work", we report both the sentences to be replaced and the replacement.

ABSTRACT

WRONG: "In the G24 C core, water maser spots show very fast (100–200 km s^{-1}) and nearly parallel proper motions, which might indicate that the water maser emission is tracing a collimated jet."

CORRECTED: "In the G24 C core, water maser emission emerges from separated clusters of features, and the measured feature proper motions suggest that in each cluster water masers trace outflowing motion from a different YSO."

3.4.4. Cluster "C"

The VLBA maser cluster "C" is located close to the center of the mm core C. We identified 117 maser features and measured proper motions for 23 of them, whose emission was persistent over three or four epochs. While towards core A water maser emission is detected across a LSR velocity range within ±20 km s^{-1} from $V_{\rm sys}$ ($|V_{\rm LSR}-V_{\rm sys}| \leq 20$ km s^{-1}), towards core C water features emit across a much larger range of blueshifted velocities, extending up to ≈80 km s^{-1} below $V_{\rm sys}$. Based on the spatial and the 3D velocity distribution of the maser features, cluster "C" can be divided into six subclusters, named "C1", "C2", ... up to "C6". Figure 4, panel C shows the water maser positions and velocities in subclusters "C1" to "C5". Subcluster "C6", including only two weak features (see Table 6), is placed ≈0.″5 to northwest of the region in panel C of Fig. 4 and is not shown here.

The "C2" subcluster presents a SE-NW elongated spatial distribution with a diameter of ≈600 AU. Features to the SE (NW) are redshifted (blueshifted) by up to ≈20 km s^{-1} with respect to $V_{\rm sys}$. The measured absolute proper motions have amplitudes between 50 and 140 km s^{-1} and indicate that features located at opposite ends of the "C2" linear distribution have divergent motions, with sky-projected directions varying by ≈150° across the subcluster.

Positions and velocities of water masers in subcluster "C1", "C3" and "C4" share some similarities. In each subcluster the strongest features are concentrated in a small area ≤100 AU in size. Measured proper motions show that maser features are moving away from each subcluster concentration with velocities ranging in amplitude between 10 and 50 km s^{-1} (see Table 6) and directed across a large opening angle. In each of the three subclusters, water masers concentrate in a different range of LSR velocities. Water maser emission in subcluster "C1" extends across the $V_{\rm LSR}$ interval 114–127 km s^{-1}, masers in subcluster "C3" emit mainly in the $V_{\rm LSR}$ range 40–80 km s^{-1}, the subcluster "C4" maser emission covers the interval 80–100 km s^{-1}.

The subcluster "C5" is composed by a few, sparse maser features distributed across an area of ≈1000 AU in diameter southward of the water maser distribution in core "C". Water masers of this subcluster have LSR velocities within ±7 km s^{-1} from $V_{\rm sys}$. Proper motions are measured only for two features, which move concordly towards N-NW with amplitudes of about 40 km s^{-1}.

⋆ Table 6 is only available in electronic form at http://www.aanda.org

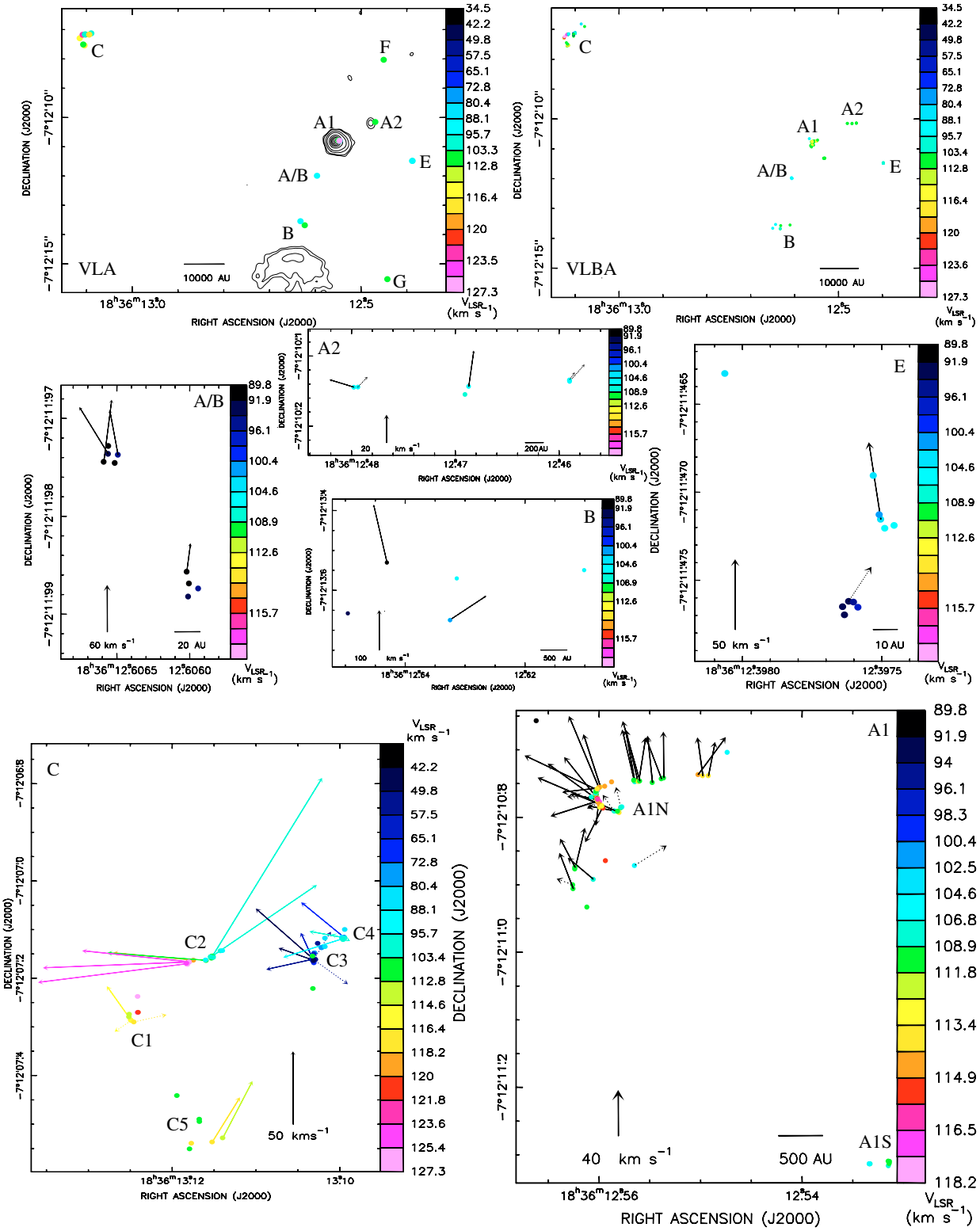

Fig. 4. Position and velocities of the water maser features detected with VLA and VLBA. *Upper panels: the left and right upper panels* show the spatial distribution of the maser features detected using respectively the VLA and the VLBA arrays. The contour map in the left upper panel shows the three continuum sources (A1, A2 and B) detected towards the G24 core with the VLA-B array in the 1.3 cm band. The dot *colors* denote different LSR velocities, according to the scale on the right-hand side of the panels. The VLA and/or VLBA maser emission originates from distinct centers, labelled with the letters "A1", "A2", "A/B", "B", "C", "E", "F", and "G". VLA regions "F" and "G", falling too distant ($\geq 3''$) from the VLBA correlator position towards the mm core A, are not mapped with the VLBA. *Middle and lower panels: middle and lower panels* show the detailed spatial and velocity distribution of the maser features detected in each of the six VLBA maser clusters. Each panel is named after the maser cluster to which it refers. Different *colors* indicate the variation of the maser LSR velocities, according to the colour scale on the right-hand side of the panel. The measured feature absolute proper motions are indicated with arrows, using dotted arrows to denote the most uncertain measurements; the proper motion amplitude scale is given at the bottom of each panel. *Lower panels* show that the VLBA maser clusters "A1" and "C" can be further sorted into subclusters "A1N" and "A1S", and subclusters "C1", "C2", "C3", "C4" and "C5" respectively.

6. Water maser outflows in the G24 C mm core

Towards the G24 C mm core, no radio continuum emission in the 1.3 cm and 7 mm bands has been detected by recent sensitive[1] VLA observations (Beltrán et al. 2007), which indicates that either YSOs in this core have a spectral type later than B2 or they are in an early evolutionary stage prior to the appearance of an HII region. The low gas temperatures of ≈30 K derived using the NH_3 line (Codella et al. 1997) may explain the non-detection of the Class II 6.7 GHz masers in this core, since excitation models predict these masers to be radiatively excited and reach high brightness temperatures for kinetic temperatures of ≈150 K (Cragg et al. 2005). The detection of the Class I 44 GHz and 95 GHz maser clusters in correspondence of the peak of the CS(3–2) map and roughly at the center of the ^{12}CO(1–0) bipolar outflow (see Fig. 1), is consistent with the idea that the Class I methanol masers are collisionally excited in shocks propagating through dense ambient gas.

The spatial and velocity distribution of water maser features in subclusters "C1", "C2", "C3" and "C4" suggests that in each subcluster water masers trace outflowing motion from a different YSO. In the subcluster "C2", symmetry considerations would place the YSO midway of the redshifted and blueshifted features. For the other subclusters ("C1", "C3" and "C4"), the YSO exciting the maser outflow might be found at the position where the strongest features cluster. As discussed in Furuya et al. (2002), the large mass of the G24 C mm core (≈250 $M_\odot$) and the detection of molecular species such as CH_3CN, typical of hot cores, indicate that this region can harbour high-mass (proto)stars. The presence of intense outflow activity may witness the early evolutionary stage of the massive YSOs, which should be still actively accreting mass and not yet massive enough (≤8 $M_\odot$) to ionize the surrounding environment.

It is interesting to note that the outflow traced by the water masers in subcluster "C2" is both the fastest and the most collimated among the four maser outflows observed in the region. That is in qualitative agreement with the properties of the molecular outflows observed both in low- and high-mass YSOs, where the degree of collimation is observed to increase with the expansion velocity.

7. Conclusions and future work

WRONG: "In the G24 C subcore, many of the detected water maser features move fast (at velocities of ∼100–200 km s^{-1}) and along a common direction (at PA ≈ 200°), which might suggest that the water maser emission traces a collimated outflow. We plan to perform sensitive, sub-arcsecond angular resolution observations of G24 C in typical outflow tracers (like SiO and HCO^+) to inquire for the presence of (proto-)stellar outflows."

CORRECTED: "In the G24 C subcore, most of the water maser emission emerges from four separated clusters of features emitting in different V_{LSR} intervals. In each cluster, the measured proper motions appear to trace an outflow emerging from the cluster centre. We suggest that each of the maser outflows is driven by a YSO in an early, accretion phase."

[1] The channel map rms noise was 0.09 mJy beam^{-1} and 0.27 mJy beam^{-1} at 1.3 cm and 7 mm, respectively.

Table 6. Parameters of VLBA water maser features in core C. For each identified feature, Col. 1 indicates the harboring maser subcluster; Cols. 2 and 3 the LSR velocity and the integrated flux density of the highest-intensity channel; Cols. 4 and 5 the positional (RA and Dec) offsets (with the associated errors), evaluated with respect to the derived absolute position of the reference feature (α(J2000) = $18^h36^m13^s.1140$, δ(J2000) = $-7°12'7''.528$); Cols. 6–8 the projected components along the RA and Dec axes and the absolute value of the derived proper motions (together with the associated errors).

Cluster	V_{LSR} (km s^{-1})	F_{int} (Jy)	$\Delta\alpha$ (mas)	$\Delta\delta$ (mas)	V_x (km s^{-1})	V_y (km s^{-1})	V_{mod} (km s^{-1})
C5	114.5	4.8	0.0 ± 0.2	0.0 ± 0.2	−18 ± 9	39 ± 9	43 ± 9
C5	110.8	1.3	81.2 ± 0.2	87.0 ± 0.2			
C5	107.7	1.1	41.2 ± 0.2	33.5 ± 0.2			
C5	116.7	0.8	18.6 ± 0.2	−8.4 ± 0.2	−16 ± 18	31 ± 19	35 ± 19
C5	117.9	0.2	55.1 ± 0.2	−10.7 ± 0.2			
C5	107.6	0.1	58.7 ± 0.2	−22.5 ± 0.2			
C5	107.2	0.06	40.6 ± 0.2	37.9 ± 0.2			
C1	114.7	1.5	162.4 ± 0.2	241.3 ± 0.2	10 ± 10	−8 ± 10	12 ± 10
C1	115.1	0.8	163.3 ± 0.2	242.6 ± 0.2	14 ± 18	23 ± 19	27 ± 19
C1	114.2	0.3	165.9 ± 0.2	254.2 ± 0.2			
C1	114.1	0.3	166.0 ± 0.2	249.1 ± 0.2			
C1	116.5	0.2	157.6 ± 0.2	238.3 ± 0.2	−19 ± 18	5 ± 20	20 ± 19
C1	121.5	0.1	150.0 ± 0.2	257.0 ± 0.2			
C1	123.8	0.07	150.4 ± 0.2	258.1 ± 0.2			
C1	127.1	0.06	150.0 ± 0.2	290.2 ± 0.2			
C2	102.3	1.6	20.5 ± 0.2	372.7 ± 0.2			
C2	105.0	1.6	18.4 ± 0.2	370.5 ± 0.2			
C2	124.6	1.0	59.6 ± 0.2	361.6 ± 0.2	63 ± 14	8 ± 15	64 ± 14
C2	119.3	0.9	52.0 ± 0.2	365.2 ± 0.2	48 ± 11	5 ± 11	48 ± 11
C2	124.2	0.9	63.5 ± 0.2	357.3 ± 0.3			
C2	107.3	0.9	18.4 ± 0.2	372.5 ± 0.2			
C2	109.2	0.8	17.7 ± 0.2	370.5 ± 0.2			
C2	125.5	0.7	59.2 ± 0.2	361.8 ± 0.2			
C2	125.3	0.7	63.5 ± 0.2	357.4 ± 0.2	88 ± 14	−13 ± 15	89 ± 14
C2	101.1	0.5	16.1 ± 0.2	372.7 ± 0.2			
C2	103.4	0.5	29.5 ± 0.2	364.6 ± 0.2	58 ± 19	5 ± 21	59 ± 19
C2	120.6	0.4	62.6 ± 0.2	359.6 ± 0.2			
C2	94.9	0.4	20.0 ± 0.2	372.7 ± 0.2			
C2	98.4	0.4	19.5 ± 0.2	373.0 ± 0.2			
C2	96.3	0.4	18.1 ± 0.2	373.4 ± 0.2	−62 ± 10	49 ± 13	79 ± 11
C2	124.0	0.3	60.4 ± 0.2	361.0 ± 0.2	86 ± 14	−4 ± 15	86 ± 14
C2	90.8	0.3	29.7 ± 0.2	366.0 ± 0.2			
C2	103.2	0.3	19.1 ± 0.2	372.4 ± 0.2	−65 ± 18	122 ± 20	139 ± 19
C2	97.5	0.3	19.7 ± 0.2	370.1 ± 0.2			
C2	121.7	0.3	63.2 ± 0.2	358.9 ± 0.2			
C2	101.6	0.3	16.8 ± 0.2	372.5 ± 0.2			
C2	108.0	0.2	20.3 ± 0.2	372.6 ± 0.2			
C2	106.5	0.2	18.0 ± 0.2	367.3 ± 0.2			
C2	108.7	0.2	16.3 ± 0.2	371.1 ± 0.2			
C2	106.0	0.2	18.2 ± 0.2	374.0 ± 0.2			
C2	100.5	0.2	18.0 ± 0.2	372.4 ± 0.2			
C2	124.9	0.2	62.5 ± 0.2	356.8 ± 0.2			
C2	97.8	0.1	15.0 ± 0.2	368.9 ± 0.2			
C2	106.8	0.1	19.7 ± 0.2	372.7 ± 0.2			
C2	125.7	0.1	62.7 ± 0.2	358.8 ± 0.2			
C2	97.1	0.1	3.3 ± 0.2	385.1 ± 0.2			
C2	126.5	0.1	63.8 ± 0.2	355.5 ± 0.2			
C2	91.4	0.09	17.5 ± 0.2	372.5 ± 0.3			
C2	95.1	0.08	−1.3 ± 0.2	382.9 ± 0.2			
C2	119.6	0.07	61.3 ± 0.2	361.2 ± 0.2			
C2	107.9	0.05	17.4 ± 0.2	373.1 ± 0.2			

Table 6. continued.

Cluster	$V_{\rm LSR}$ (km s^{-1})	$F_{\rm int}$ (Jy)	$\Delta\alpha$ (mas)	$\Delta\delta$ (mas)	V_x (km s^{-1})	V_y (km s^{-1})	$V_{\rm mod}$ (km s^{-1})
C3	54.0	59.9	−161.0 ± 0.2	364.7 ± 0.2	−10 ± 21	20 ± 21	22 ± 21
C3	60.8	16.4	−160.0 ± 0.2	366.9 ± 0.2	7 ± 11	18 ± 12	19 ± 12
C3	48.9	11.8	−161.8 ± 0.2	364.0 ± 0.2			
C3	56.3	7.2	−160.7 ± 0.2	366.8 ± 0.2	28 ± 15	−7 ± 17	28 ± 15
C3	57.2	6.0	−161.0 ± 0.2	365.2 ± 0.2			
C3	73.0	4.0	−163.0 ± 0.2	380.2 ± 0.2			
C3	43.8	3.1	−161.4 ± 0.2	365.3 ± 0.2			
C3	43.0	2.4	−160.5 ± 0.2	365.9 ± 0.2			
C3	57.1	2.3	−161.5 ± 0.2	364.1 ± 0.2			
C3	48.8	1.2	−161.8 ± 0.2	364.8 ± 0.2	21 ± 14	9 ± 15	22 ± 14
C3	44.0	1.0	−160.1 ± 0.2	366.3 ± 0.2			
C3	47.9	0.9	−162.3 ± 0.2	366.5 ± 0.2	34 ± 15	35 ± 15	49 ± 15
C3	39.5	0.8	−161.4 ± 0.2	365.6 ± 0.2			
C3	109.6	0.8	−161.4 ± 0.2	371.7 ± 0.2			
C3	88.1	0.7	−161.0 ± 0.2	374.1 ± 0.2			
C3	37.8	0.7	−160.7 ± 0.2	366.8 ± 0.2			
C3	58.2	0.6	−162.8 ± 0.2	361.7 ± 0.2			
C3	56.1	0.6	−158.8 ± 0.2	368.6 ± 0.2	−21 ± 20	−18 ± 23	28 ± 21
C3	116.6	0.5	−160.1 ± 0.2	365.3 ± 0.2			
C3	105.2	0.5	−159.2 ± 0.2	367.1 ± 0.2			
C3	58.0	0.4	−160.4 ± 0.2	365.1 ± 0.2			
C3	99.6	0.3	−159.8 ± 0.2	366.1 ± 0.2			
C3	34.6	0.3	−161.0 ± 0.2	368.0 ± 0.2			
C3	64.4	0.3	−160.5 ± 0.2	366.5 ± 0.2			
C3	76.7	0.3	−176.3 ± 0.2	390.4 ± 0.2			
C3	42.1	0.3	−163.0 ± 0.2	365.8 ± 0.2			
C3	52.1	0.3	−162.5 ± 0.2	362.1 ± 0.2			
C3	70.3	0.2	−162.4 ± 0.2	359.9 ± 0.2			
C3	49.9	0.2	−164.8 ± 0.2	366.0 ± 0.2			
C3	42.0	0.2	−162.6 ± 0.2	365.3 ± 0.2			
C3	74.0	0.2	−175.8 ± 0.2	390.1 ± 0.2			
C3	68.3	0.2	−162.8 ± 0.2	379.9 ± 0.2			
C3	68.9	0.2	−161.4 ± 0.2	364.2 ± 0.2			
C3	54.8	0.2	−162.5 ± 0.2	361.7 ± 0.2			
C3	45.3	0.2	−162.5 ± 0.2	365.5 ± 0.2			
C3	105.6	0.2	−160.3 ± 0.2	365.6 ± 0.2			
C3	39.5	0.1	−161.4 ± 0.2	366.7 ± 0.2			
C3	43.4	0.1	−163.3 ± 0.2	363.5 ± 0.2			
C3	52.6	0.1	−165.3 ± 0.2	366.9 ± 0.2			
C3	78.5	0.1	−163.3 ± 0.2	380.6 ± 0.2			
C3	48.0	0.1	−162.0 ± 0.2	364.3 ± 0.2			
C3	50.6	0.1	−160.9 ± 0.2	365.9 ± 0.2			
C3	38.0	0.08	−161.3 ± 0.2	365.9 ± 0.2			
C3	105.5	0.08	−161.2 ± 0.2	306.5 ± 0.2			
C3	62.4	0.05	−163.6 ± 0.2	376.3 ± 0.2			
C3	53.8	0.05	−169.6 ± 0.2	399.3 ± 0.2			

Table 6. continued.

Cluster	$V_{\rm LSR}$ (km s^{-1})	$F_{\rm int}$ (Jy)	$\Delta\alpha$ (mas)	$\Delta\delta$ (mas)	V_x (km s^{-1})	V_y (km s^{-1})	$V_{\rm mod}$ (km s^{-1})
C4	96.9	2.4	−215.6 ± 0.2	410.3 ± 0.2	−4 ± 10	−2 ± 10	4 ± 10
C4	97.0	1.6	−215.1 ± 0.2	405.9 ± 0.2			
C4	83.1	1.4	−212.6 ± 0.2	409.5 ± 0.2			
C4	94.8	0.9	−216.5 ± 0.2	406.7 ± 0.2			
C4	96.0	0.8	−216.9 ± 0.2	407.1 ± 0.2			
C4	100.1	0.5	−216.8 ± 0.2	410.9 ± 0.2	21 ± 14	4 ± 18	21 ± 14
C4	71.0	0.5	−215.6 ± 0.2	412.4 ± 0.2	25 ± 14	24 ± 15	35 ± 14
C4	98.1	0.3	−211.9 ± 0.2	410.9 ± 0.2	6 ± 18	2 ± 19	7 ± 18
C4	95.4	0.3	−214.0 ± 0.2	409.0 ± 0.2	35 ± 15	−13 ± 15	38 ± 15
C4	80.4	0.2	−214.9 ± 0.2	409.6 ± 0.2			
C4	96.9	0.2	−216.8 ± 0.2	411.4 ± 0.2			
C4	87.7	0.2	−182.0 ± 0.2	392.3 ± 0.2			
C4	82.7	0.2	−215.9 ± 0.2	412.6 ± 0.2			
C4	97.7	0.1	−215.8 ± 0.2	406.0 ± 0.2			
C4	84.5	0.1	−182.5 ± 0.2	410.0 ± 0.2			
C4	83.5	0.1	−214.7 ± 0.2	411.0 ± 0.2			
C4	82.2	0.07	−216.7 ± 0.2	428.4 ± 0.2			
C4	90.1	0.06	−212.3 ± 0.2	412.8 ± 0.2			
C6	109.9	0.8	−536.0 ± 0.2	629.0 ± 0.2			
C6	85.2	0.04	−421.3 ± 0.2	715.4 ± 0.3			